Open Ceramics 26 (2026) 100972

Contents lists available at ScienceDirect

Open Ceramics

journal homepage: www.sciencedirect.com/journal/open-ceramics

Green synthesis of diopside from hazardous waste: crystal structure and applications

Alessandro F. Gualtieri [a], Francesco Colombo [a,*], Luca Nodari [b], Enrico Mugnaioli [c,d], Iryna Andrusenko [d], Andrea Orlando [e], Eleonora Braschi [e], Riccardo Fantini [a]

[a] Department of Chemistry and Geological Sciences, University of Modena and Reggio Emilia, 41125 Modena, Italy
[b] CNR-ICMATE, 35127 Padova, Italy
[c] Department of Earth Sciences, University of Pisa, 56126 Pisa, Italy
[d] Center for Instrumentation Sharing of the University of Pisa (CISUP), University of Pisa, 56126 Pisa, Italy
[e] C.N.R.– I.G.G.– U.O.S., 50121 Florence, Italy

ARTICLE INFO

Keywords:
Diopside
Green synthesis
Recycling
Ceramics
Crystal-structure

ABSTRACT

A green and efficient route to synthesize pure diopside using recycled hazardous mineral wool waste is presented, marking the first successful transformation of this waste into a valuable ceramic material. Hazardous mineral wool undergoes industrial thermal inertization to form an inert glass (Re.Wo) to be used at up to 40 wt.% in the diopside formulation. Chemical-grade reagents generally used for the diopside synthesis are replaced by waste and natural raw materials. Unlike other waste-based approaches, this method requires no energy-intensive pre-treatments and avoids CO_2-emitting inputs. The resulting diopside exhibits broad application potential, including biomedical devices, low-expansion dielectric ceramics, photo-catalysis, and environmental remediation—leveraging transition metals within the crystal structure to enhance catalytic performance. Importantly, the process also immobilizes hazardous elements (e.g., Cr) without generating carcinogenic crystalline silica phases, offering both environmental and functional advantages.

1. Introduction

Diopside, ideally $MgCaSi_2O_6$, is a common rock-forming mineral that belongs to the pyroxene group of silicates characterized by single chains of Si-centred tetrahedra [1,2]. Diopside crystallizes in the monoclinic system with space group $C2/c$ ($Z = 4$) and unit cell parameters $a = 9.746$ Å, $b = 8.899$ Å, $c = 5.251$ Å and β=105.63° [2]. Diopside displays two distinct cation sites: M1, namely occupied by Mg^{2+}, which is 6-fold co-ordinated by oxygen atoms, and M2, namely occupied by Ca^{2+}, which is in a more irregular polyhedron with 6–8 oxygen neighbours. Diopside can form complete solid solutions with hedenbergite ($FeCaSi_2O_6$) and augite ($(Mg, Fe)CaSi_2O_6$), as well as partial solutions with orthopyroxenes and pigeonite ($(Mg, Fe)_2Si_2O_6$) [3].

Natural or synthetic diopside based raw materials have several novel high-value industrial or technological applications [4,5]. Due to its biocompatibility, bioactivity and stability, use of diopside in biomedical applications is very promising [6]. Diopside forms a Ca-rich layer on its surface when implanted in body fluids, which promotes bonding with natural bones. In dental applications, diopside has a role in restorative materials and bioactive glass pastes, where it can re-mineralize enamel and bond with dentin. Diopside has also been used for the preparation of bio-ceramic composites. In combination with hydroxyapatite, ideally $Ca_5(PO_4)_3(OH)$, or other bio-ceramics, diopside can improve mechanical strength and biodegradability, tailoring materials for specific clinical applications [7]. In metallurgy, diopside can be used in the formulation of synthetic slags in the steel industry [8]. Diopside can undergo mineral carbonation making it a candidate for carbon capture and storage [9]. Diopside can also be used as active filler into geopolymer matrices, improving mechanical strength and durability, thermal resistance, and resistance to chemical attacks [10]. Finally, diopside is one of the main phases formed after the devitrification of Mg-Ca-based glass ceramics [8,11,12].

To the knowledge of the authors, natural diopside of commercial grade is only mined and marketed in China and gem-stone quality Cr-rich diopside is mined in limited amounts in Siberia (Russia) [13]. Usually, diopside is synthesized with the melting method [14] starting from a weighed mix of natural or chemical grade reagents such as calcite ($CaCO_3$), lime (CaO), portlandite ($Ca(OH)_2$), dolomite ($CaMg(CO_3)_2$),

* Corresponding author.
E-mail address: francesco.colombo@unimore.it (F. Colombo).

https://doi.org/10.1016/j.oceram.2026.100972
Received 16 December 2025; Received in revised form 6 May 2026; Accepted 8 May 2026
Available online 9 May 2026

periclase (MgO), brucite ($Mg(OH)_2$) and a silica (SiO_2) source, namely quartz.

In the last decade, in response to the crisis of the outdated economic linear model, driven by the need of sustainability and to address growing resource paucity, the concept of the so-called "Circular Economy" has vigorously emerged [15]. A shift towards a "waste-to-value" model, where waste is recycled as secondary raw material for various production processes, thereby increasing the value of waste [16], is promoted. In this scenario, green synthesis using recycled wastes instead of natural raw materials involves creating new products from wastes. Among the benefits, it reduces pollution, minimizes landfill waste, conserves natural resources, creates new value from waste materials, potentially reducing costs associated with waste management and raw material consumption [17]. Recently, the possibility of exploiting the product of thermal inertization of hazardous mineral wool waste in the production of traditional ceramics was demonstrated [18]. Mineral wool has been used for about 50 years in a wide range of building materials such as home furniture, thermal and acoustic insulation. After the ban of asbestos, mineral wool became one of the most represented substitutes in this class of materials [19]. Mineral wool is a potential health risk to humans because, especially the batches produced before 2002, may contain respirable fibres [20] that can persist in the lungs if the wool is high in silica and low in alkalis. Nowadays, mineral wool waste is often the result of demolition of old buildings and, according to the European waste catalogue (EWC), this typology of waste is classified as other insulation materials consisting of or containing hazardous substances with code *17 06 03** [21]. For this reason, hazardous mineral wool waste must be removed and disposed of in dedicated landfills. The thermal inertization of this hazardous waste represents a practicable alternative to landfilling. Patented in 2021 [22], this process comprises oxy-combustion at 1250–1350 °C to melt the pristine fibrous wool into an inert non-fibrous obsidian-like glass that can be recycled as secondary raw material. In Arletti et al. [18] it has been demonstrated that this secondary raw material (the so called Recycling Wool Re.Wo) is basically a glass to be used as a frit in the manufacture of traditional ceramics.

This work describes the novel green synthesis of diopside starting from the secondary raw material Re.Wo, obtained by the thermal inertization of hazardous mineral wool, mixed with other low cost natural raw materials. A comprehensive description of the crystal-structure of the pure product is described together with possible future applications in ceramic products.

2. Materials and methods

The secondary raw material Re.Wo was obtained from hazardous rock wool in two main steps: (1) pressed big-bags of rock wool sealed with polyethylene are melted at 1250 °C using a propane melting furnace; (2) the molten material is rapidly cooled by quenching in a water bath, to avoid crystallization [18,22]. The Re.Wo chemical composition, expressed as major wt.% oxides, is: SiO_2= 45.2; Al_2O_3=12.9; CaO=16.1; MgO=10.2; Fe_2O_3=9.67; Na_2O=3.55; TiO_2=1.24; K_2O=0.73; MnO=0.23; P_2O_5=0.17 [18]. The synthesis of diopside requires to approach its ideal chemical composition, basically SiO_2= 55.49 wt.%; CaO=25.9 wt.%, and MgO=18.61 wt.%. To do so, the following raw materials were used to prepare the mixes in addition to Re.Wo: a commercial natural wollastonite ($CaSiO_3$) from Willsboro (New York, USA) with SiO_2=48.3 wt.% and CaO=51.7 wt.%; a commercial natural olivine ($(Mg, Fe)_2SiO_4$) from Finero (Italy) with SiO_2=41.3 wt.%, MgO=50.1 wt.% and FeO=8.6 wt.%; a commercial natural quartz (SiO_2) from Dordogne (France) with SiO_2=99.9 wt.%. A number of experiments were attempted to find the best composition and optimize the experimental conditions. For each composition, the raw materials were mixed to obtain 200 g of dry mix. The mixes were ball milled in a porcelain jar using 200 g of dense alumina grinding balls and 50 wt.% of water (by weight of the dry mix) for 10 min. The slurries were then dried at 105 °C for 24 h. The obtained powders were put in alumina refractory crucibles and fired following the solid-state synthesis route. The firing curve included 20 °C/min heating ramp, isotherm at 1300 °C for 1 h and 20 °C/min cooling step. The best composition for the synthesis of diopside was 40 wt.% Re.Wo, 34 wt.% wollastonite, 22 wt.% olivine and 4 wt.% quartz.

Preliminary optical observation of the synthetic crystals of the diopside sample was done with a Meiji Techno stereomicroscope (50 ×). Scanning electron microscope (SEM) experiments were conducted using a JSM-6010PLUS/LA (JEOL, Hillsboro, OR, USA) equipped with an energy-dispersive X-ray spectrometer (EDS) Oxford INCA-350 microanalysis system. Fragments of the sample were mounted on an Al stub and coated using a Balzers CED-010 carbon coater (10 nm thick).

TEM analysis was performed with a JEOL JEM F200 Multipurpose TEM, working at 200 kV and equipped with a Schottky field emission gun (FEG). A small tip of sample (about 20 mg) was dispersed in 40 ml of ethanol and sonicated for 2 s. Then, two drops of the suspension were placed on a carbon coated Cu TEM grid. EDS and electron diffraction were performed in scanning transmission electron microscopy (STEM) mode. Images were acquired by a high-angle annular dark-field (HAADF-STEM) mode. EDS point analyses and maps were collected with a JEOL silicon-drift detector (SDD) and analysed with JEOL Analysis Station software. Electron diffraction data were collected with a beam size of about 30 nm in diameter, obtained using the highest probe size and by inserting a 10 μm C2 condenser aperture, and recorded by an ASI CheTaah hybrid-pixel electron detector (512 × 512 pixels). Limited to pyroxene, three-dimensional electron diffraction (3DED) [23] data were collected in a tilt range of ±25° to confirm the cell parameters of the selected crystals.

The X-Ray powder diffraction (XRPD) patterns for the qualitative phase analysis of the synthesis products and structure refinement of the diopside sample were accomplished using a θ–θ Bragg-Brentano PANalytical *'XPert Pro* Diffractometer equipped with a Cu Kα radiation tube operating at 40 kV and 40 mA and with a real time multiple strip (RTMS) detector. The raw sample was ground in agate shutter box for 15 min and finely powdered using an agate mortar. Data were collected in the angular range 3–80 ° 2θ for the qualitative phase analysis and 3–120 ° 2θ for the Rietveld structure refinement using step scan of 0.0167 ° 2θ and a counting rate of 12 and 250 s/step, respectively. A 0.5° divergence slit and 0.04 rad Soller slits were used for both measurements. The XRPD patterns were analysed using the *X-Pert High Score Plus* suite. The structure refinement with the Rietveld method was conducted using the EXPGUI interface [24] of the GSAS package [25]. Starting structure model was taken from Cameron et al. [26]. The site occupancies of the M1 and M2 sites were kept fixed to the values measured with the electron probe microanalysis (EPMA) (see below).

Room temperature Mössbauer spectroscopy data were performed using a constant acceleration spectrometer mounting a Rh matrix ^{57}Co source, nominal strength 1850 MBq. The spectrum of the sample was collected by placing ≈ 80 mg of grinded powder dispersed in petrol jelly in a 17 mm diameter sample holder. The obtained spectrum was fitted to Lorentzian line shapes using a minimum number of sextets and doublets. The obtained hyperfine parameters, isomer shift (δ), quadrupole splitting (Δ), half linewidth at half maximum (Γ^+), are expressed in mm/s, while the relative areas (A) in %. The velocity was calibrated against a α-Fe foil and δ is quoted relative to metallic iron at room temperature. The results of the Mössbauer experiments allowed us to calculate the fraction of Fe^{2+} and Fe^{3+} to integrate the chemical data for the calculation of the diopside chemical formula.

Major and minor element contents of the sample were measured by electron probe microanalysis (EPMA) on a polished section prepared with several diopside crystals embedded in epoxy resin. The instrument is a JEOL Superprobe JXA-8230, equipped with five wavelength-dispersive spectrometers operating with different diffracting crystals and detectors (gas flow and sealed Xe type). The analytical conditions were 15 kV accelerating voltage, 20 nA beam current, and 3 μm beam

diameter. A ZAF data correction model was used to get quantitative results. Standardizations were performed on Astimex and Smithsonian (only for Fe and Ti) standards.

3. Results and discussion

The synthesis of pure diopside has been accomplished via high temperature melting and solid-state crystallization. The synthesis was performed at 1300 °C for 1 h, using 40 wt.% of a secondary raw material obtained by the melting at 1250 °C of hazardous mineral wool, mixed with other low-cost natural raw materials (34 wt.% wollastonite, 22 wt. % olivine and 4 wt.% quartz). A strongly sintered product was obtained with crystals grown in radiating aggregates (see the microscope image in Fig. 1) resembling the pyroxene-rich symplectites [27] formed by complex solid-state recrystallization processes where diopside orientation is controlled by that of the parent phases (olivine or wollastonite here).

Beautiful aggregates of diopside crystals of various shapes have also been observed with SEM (Fig. 2). The relative EDS spectra, reported as Supporting information SI, evidences the typical elements of diopside with Si, O, Mg, and Ca as major elements and Na, Al and Fe as minor elements.

TEM data collected on a number of diopside particles, both single crystals and crystal aggregates representative of the synthetic product, showed that iron is invariably found as a component of the diopside crystalline lattice and not as iron-rich impurity. Fig. 3 depicts one of these diopside crystals with the associated EDS map, witnessing that iron is associated to the diopside crystals. The TEM investigation also allowed us to discover that a minor fraction of the sample contains an Al-rich crystalline phase which is probably a plagioclase. This phase is present in significant quantities (approx. 30 wt.%) in a peripheral portion of the synthesis product near the walls of the alumina crucible used for the synthesis. It is likely that a part of the melt, enriched in Na and hence more fluxing, in contact with the crucible, created a eutectic point with alumina that prompted diffusion of Al into the glass matrix so that a reaction halo formed at the edges of the sample containing this Al-enriched plagioclase phase. Supporting information SII reports a representative image and the associated EDS map of one of these particles showing the high content of Al and Na. The chemical composition in atoms wt.% of this phase point to a plagioclase term, ideally $Na_{2-x}Ca_{x-1}Al_xSi_{4-x}O_8$ (with $1 \leq \leq 2$). Any attempt to obtain electron diffraction data resulted in a polycrystalline pattern, suggesting that the grains of this phase are indeed very small. The poor crystallinity and the limited overall content in the sample results in a signal that is below the limit for X-Ray powder diffraction (generally estimated about 1 wt.%).

The Mössbauer spectrum (Fig. 4) shows intense absorptions in the 0–2 mm/s velocity range ascribable to the presence of paramagnetic Fe (III) and Fe(II) species. The simplest model was chosen to fit the spectrum: two doublets representing ferric sites together with one relative to ferrous one. The so-obtained hyperfine parameters are reported in Supporting information SIII Table. The ferric population, comprising approximately 86% of the total iron content, is distributed across two sites: site 1, representative of Fe(III) in a distorted octahedral environment (M sites), and site 2, representative of Fe(III) in a distorted tetrahedral environment (T sites). The remaining Fe, in form of Fe(II), occupies a single distorted octahedral site (M sites). The data obtained are in line with those obtained by Redhammer et al. [28] in Mg rich samples, and therefore near the diopside in the solid solution.

The EPMA data were collected on 29 crystals representative of synthetic diopside. All the collected point analyses are reported in Supporting information SIV Figure. Only 2 outliers were removed and the chemical formula was calculated on the basis of 6 oxygen atoms, following the scheme proposed for the nomenclature of pyroxenes by Morimoto et al. [29] (see the calculation sheet in Supporting information SIV Table). The speciation of Fe(III) and Fe(II) from the Mössbauer data was used to distribute the iron content and assign the two iron species to octahedral (M) and tetrahedral sites. The calculated chemical formula is given below.

$$(Ca_{0.941}Na_{0.032}Mg_{0.027})(Mg_{0.822}Fe^{3+}_{0.097}Al_{0.045}Fe^{2+}_{0.02}Ti_{0.008}Cr_{0.005}Mn_{0.003})(Si_{1.863}Al_{0.111}Fe^{3+}_{0.026})O_6$$

With the Mössbauer and EPMA data, it was possible to confirm that the synthetic material can be classified as diopside, according to the nomenclature of pyroxenes [29] and to refine the structure model from the XRPD data. The graphical output of the Rietveld refinement performed with GSAS [25] is reported as Supporting information SV. All the refinement statistics of the Rietveld refinement, witnessing the goodness of the fit, are reported as GSAS output in Supporting information SV. The calculated unit cell parameters are $a = 9.7469(2)$ Å; $b = 8.9034(2)$ Å; $c = 5.2740(1)$ Å; $\beta = 105.993(1)°$. The atom positions, occupancies, and atomic displacement factors calculated from the structure refinement and relative errors in parenthesis are reported in Table 1. No errors are reported on the site occupancies because the values were fixed from the calculated chemical formula. Supporting information SV Table contains the most significant calculated bond distances from the structure

Fig. 1. Synthetic diopside product showing radiating aggregates resembling those observed in the natural rock symplectites.

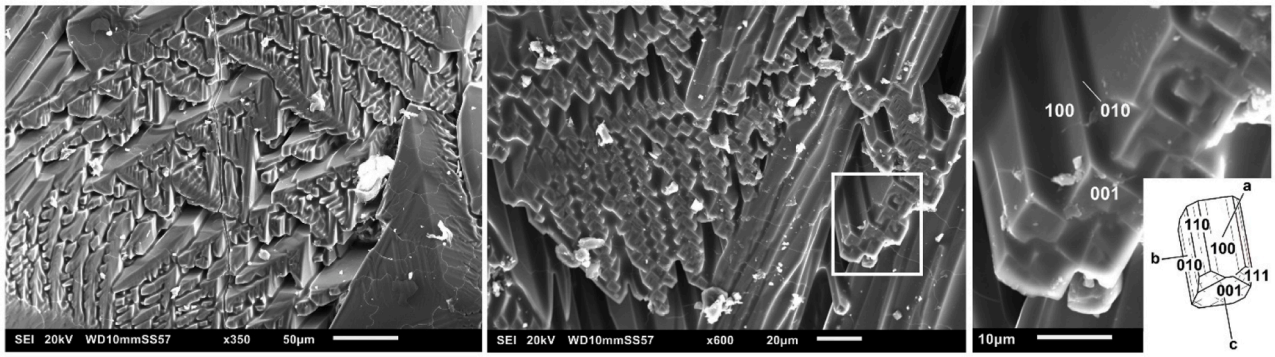

Fig. 2. SEM images of synthetic Diopside crystals of various shapes. The relative EDS spectra are reported as Supporting information SI. The right figure is a zoom of the central figure (white inset) reporting the crystal form of the pyroxene crystals and relative indexing of the main crystal faces (100), (010) and (001).

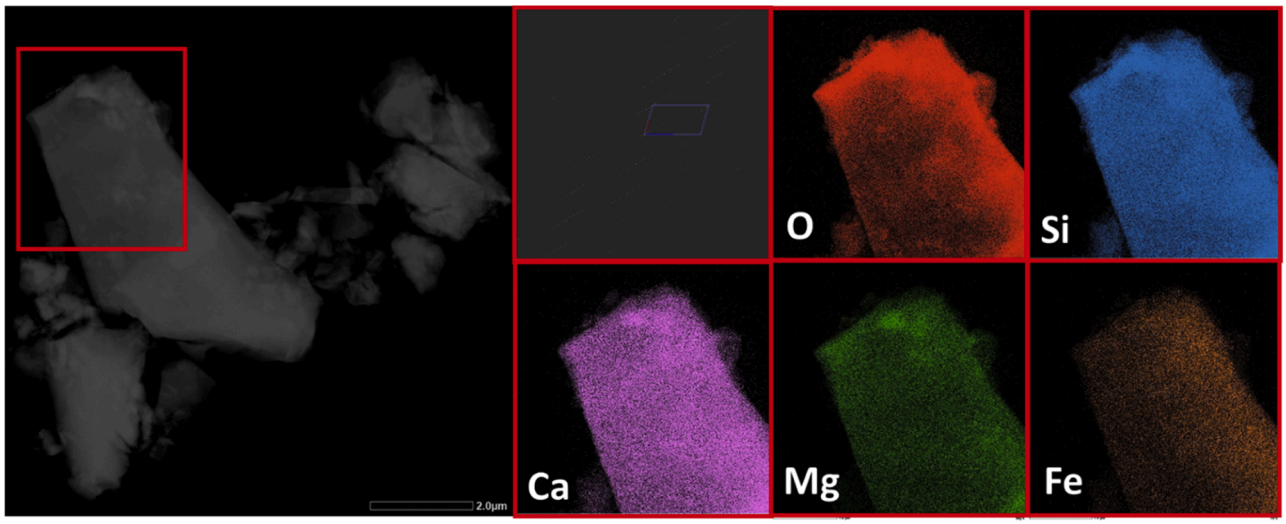

Fig. 3. STEM image of a diopside crystal representative of the synthetic product, and associated 3DED volume with superimposed the sketch of the unit cell and the EDS map showing that iron is a component of the diopside crystalline lattice and not a separate iron-rich impurity in the sample.

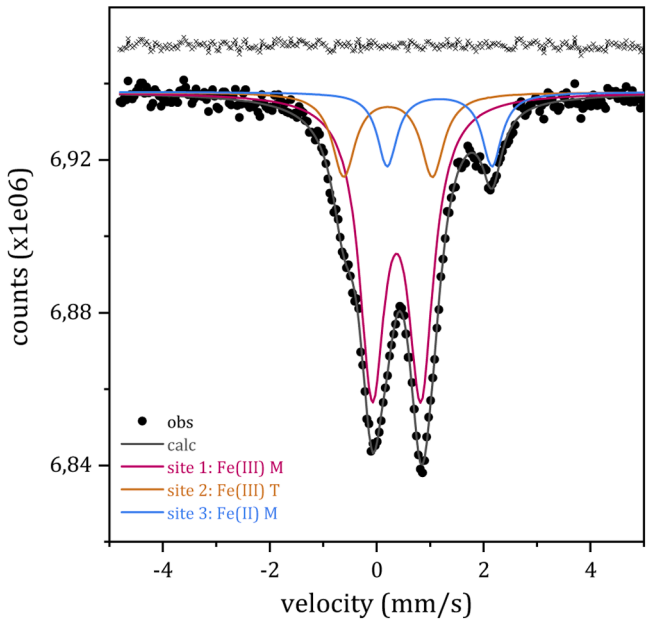

Fig. 4. The Mössbauer spectrum of synthetic diopside showing the chemical environment of the iron species.

Table 1
Calculated atom positions, occupancies, and atomic displacement factors (Å^2) of synthetic diopside.

Site	Occupancy	*x*	*y*	*z*	U_{iso}(Å^2)
M1	0.822 Mg^{2+} 0.097 Fe^{3+} 0.045 Al^{3+} 0.02 Fe^{2+} 0.008 $Ti4^{+}$ 0.005 Cr^{3+} 0.003 Mn	0	0.9074(2)	0.25	0.019(1)
M2	0.941 Ca^{2+} 0.032 Na^{+} 0.027 Mg^{2+}	0	0.3001(2)	0.25	0.0237(9)
T	0.9315 Si^{4+} 0.0515 Al^{3+} 0.013 Fe^{3+}	0.2878(2)	0.0919(2)	0.2302(4)	0.017(1)
O1	1	0.1164(2)	0.0859(3)	0.1438(6)	0.0296(9)
O2	1	0.3634(3)	0.2507(3)	0.3205(7)	0.039(1)
O3	1	0.3464(3)	0.0157(3)	0.9906(6)	0.01053

refinement.

A plot of the refined structure model is shown in Fig. 5 with the tetrahedra arranged in chains that extend along the *c* axis. Si and minor Al and Fe^{3+} occupy 4-fold coordination sites T. The calculated mean T-O distance is 1.6306 Å. The tetrahedral chains (in yellow in Fig. 5) are linked together mostly by Ca and Mg ions. The smaller M1 sites (red

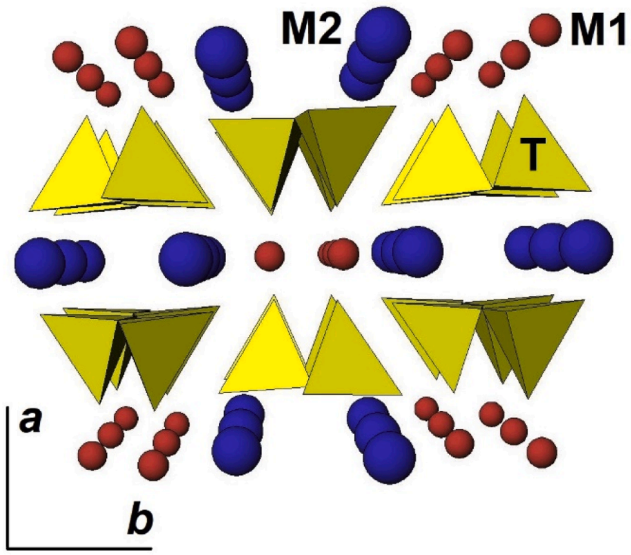

Fig. 5. A plot of the calculated structure model of diopside along the *c* axis.

balls in Fig. 5) are octahedrally coordinated by six oxygen atoms and occupied, in decreasing order of site population, by Mg^{2+}, Fe^{3+}, Al^{3+}, Fe^{2+}, $Ti4^{+}$, Cr^{3+} and Mn. The larger distorted M2 sites (blue balls in Fig. 5) are coordinated by 6–8 oxygen atoms and occupied, in decreasing order of site population, by Ca^{2+}, Na^{+}, and Mg^{2+}. The calculated mean M1-O and M2-O distances are 2.0743 and 2.5085 Å, respectively.

The comparison of our structure model with the literature crystallographic data on synthetic and natural diopside structures (Supporting information SVI reporting the mean value and relative standard deviation $a = 9.7280$ (0.0296) Å, $b = 8.9026$ (0.0260) Å, $c = 5.2527$ (0.0075) Å, $\beta = 106.0323$ (0.2990)°, T-O = 1.6346 (0.0040) Å, M1-O = 2.0718 (0.0160) Å, and M2-O = 2.4982 (0.0087) Å) evidences that the calculated unit cell, β angle, and T-O and M-O distances are within the standard deviations of the literature data except for the *c* axis which is slightly greater. It is plausible that the reason for the longer *c* (and *a*) axis length is due to the Al content in our sample. In fact, Hu et al. [30] showed that an Al-rich diopside sample has comparable length of *b* axis and β angle but longer length of *a* and *c* axes than a diopside sample with composition close to ideal one (Table 1 in [30]).

Supporting information SVI also reports the plots of the values from the literature vs. our calculated values (in red in the SVI Figures).

The innovative character of this work is that the green synthesis was carried out by recycling, for the first time, a raw material obtained from hazardous waste mineral wool. Moreover, our synthesis process differs from those described in the literature for other reasons: (i) the product of the synthesis is a single phase material, while the synthetic diopsides used in ceramics are generally mixed with other Ca-Mg-silicates like wollastonite, anorthite, gehlenite, silica polymorphs and many more (see for example [31–33]); (ii) most of the diopside synthesis in the literature is accomplished starting from chemical grade reagents and not from waste (see for example [34–36]); (iii) cases of synthesis of pure diopside using waste materials (e.g. egg shells) do exist but required preliminary energy-intensive mechanical milling [37] or thermal activation [38,39]; (iv) diopside synthesis was obtained without reagents, natural raw materials or waste containing CO_2 which is eventually released during the synthesis process (see for example [37]).

The green pure synthetic diopside synthesized here can be successfully used for a number of industrial applications:

-in electronics where diopside is used in low-expansion, dielectric ceramics and specially developed glasses;

-in photocatalysis and environmental remediation. To this aim, the catalytic and photocatalytic activity of our diopside crystal should be very promising because of the presence in the lattice of transition metals, such as Fe^{3+} and Mn. In fact, it is known that diopside catalytic performances increase with increasing dopant concentration [40];

-in traditional ceramics (e.g. tiles) to promote sintering of the ceramic body or as pigment, if doped with chromophore transition metals such as Co [31];

-after further investigation on the effects of minor and traces elements present in the material, and once industrial-scale production is established, in bio-med applications as it is non-toxic and well-tolerated by bone cells, promotes formation of hydroxyapatite layer in body fluids (like SBF) and supports osteogenesis, angiogenesis, and cell proliferation [39].

4. Conclusions

This work demonstrates a sustainable, efficient, and versatile method for obtaining pure synthetic diopside with broad application potential. For the first time, pure diopside was produced by recycling a hazardous waste (mineral wool). Pristine mineral wool underwent thermal inertization in an industrial plant into an inert glass (Re.Wo) that was included as much as 40 wt.% in the diopside formulation. The synthesis avoids the use of chemical-grade reagents, relying solely on waste and natural raw materials. Unlike other waste-based syntheses, this approach does not require energy-intensive pre-treatments such as mechanical milling or thermal activation. No reagents or raw materials containing CO_2 were used. This product can potentially be used in biomedical applications, low-expansion dielectric ceramics/glasses, photocatalysis/environmental remediation (taking advantage of the presence of transition metals in the crystal lattice that enhance catalytic activity), and traditional ceramics. Other advantages of the method are that obtained diopside crystal structure efficiently captures hazardous elements like Cr from the pristine hazardous solid waste and no secondary crystalline silica (that are classified as *Group 1* carcinogens in the respirable forms by the International Agency for Research on Cancer) phases are formed during the synthesis. However, to employ the synthesised diopside in the potential application fields mentioned above, it is first necessary that the Re.Wo production plant, currently in its start-up phase, becomes fully operational. Furthermore, it is important to consider that even once the plant is running, ensuring adequate compositional variability for the subsequent use of the material in the synthesis process will remain challenging. The possibility to work with large quantities of Re.Wo with adequate composition will open up the possibility to further investigate synthesis methodologies of pure diopside, tailoring the methodologies to better suit the specific requirements of each target application.

Appendix A. supporting information

Supplementary data associated with this article can be found in the online version at xxx

CRediT authorship contribution statement

Alessandro F. Gualtieri: Writing – review & editing, Writing – original draft, Supervision, Funding acquisition, Conceptualization. **Francesco Colombo:** Writing – review & editing, Formal analysis. **Luca Nodari:** Writing – review & editing, Formal analysis. **Enrico Mugnaioli:** Writing – review & editing, Formal analysis. **Iryna Andrusenko:** Writing – review & editing, Formal analysis. **Andrea Orlando:** Writing – review & editing, Formal analysis. **Eleonora Braschi:** Writing – review & editing, Formal analysis. **Riccardo Fantini:** Writing – review & editing, Formal analysis.

Declaration of competing interest

Alessandro F. Gualtieri is inventor of the European Patent EP

22,153,845.7 “Apparatus for treating waste containing mineral wool”. Inventors: I. Zanatto, A.F. Gualtieri. Filing date March 18, 2022 [ref. 22]. All the other authors declare that they have no known competing financial interests or personal relationships that could have appeared to influence the work reported in this paper.

Acknowledgements

This work was financially supported by the Project 101113855 – LIFE22-ENV-IT-LIFE ReWo co-funded by the European Union.

Supplementary materials

Supplementary material associated with this article can be found, in the online version, at doi:10.1016/j.oceram.2026.100972.

References

[1] J. Zussman, The crystal chemistry of pyroxenes and amphiboles, 1. Pyroxenes, Earth-Sci. Rev. 4 (1968) 39–67, https://doi.org/10.1016/0012-8252(68)90146-3.
[2] W.A. Deer, R.A. Howie, J. Zussman, Rock-forming minerals (2nd edition), vol. 2A, single-chain silicates, London (Longman) (1978) p. 668.
[3] M. Cameron, J.J. Papike, Structural and chemical variations in pyroxenes, Am. Min. 66 (1–2) (1981) 1–50.
[4] C. Saravanan, S. Sasikumar, Bioactive diopside ($CaMgSi_2O_6$) as a drug delivery carrier–a review, Curr. Drug Deliv. 9 (6) (2012) 583–587, https://doi.org/10.2174/156720112803529765.
[5] J. Almuhamadi, N. Karpukhina, M. Cattell, Diopside glass-ceramics for dental and biomedical applications, Adv. Sci. Tech. 96 (2014) 15–20, https://doi.org/10.4028/www.scientific.net/AST.96.15.
[6] S. Joseph, S. Swamiappan, Preparation and characterization of diopside-wollastonite composite for orthopedic application, Silicon 16 (3) (2024) 1161–1171, https://doi.org/10.1007/s12633-023-02737-4.
[7] S. Punj, N. Srivastava, M. Baranwal, K. Singh, In-vitro biological evaluation of diopside bio-ceramic synthesized from sustainable agro-food waste ashes, Silicon 14 (13) (2022) 7423–7433, https://doi.org/10.1007/s12633-021-01484-8.
[8] D.U. Tulyaganov, K. Dimitriadis, S. Agathopoulos, H.R. Fernandes, Glasses and glass-ceramics in the CaO–MgO–SiO2 system: diopside containing compositions-A brief review, J. Non-Cryst. Solids 612 (2023) 122351, https://doi.org/10.1016/j.jnoncrysol.2023.122351.
[9] B. Aguila, L. Hardee, H.T. Schaef, S. Zare, M.J.A. Qomi, J.V. Crum, J. E. Holliman Jr., E. Tajuelo Rodriguez, L.M. Anovitz, K.M. Rosso, Q.R. Miller, Emerging investigator series: kinetics of diopside reactivity for carbon mineralization in mafic–ultramafic rocks, Env. Sci.: Nano 10 (10) (2023) 2672–2684, https://doi.org/10.1039/D3EN00087G.
[10] Z. Zhao, C. Zhang, J. Li, W. Wang, H. Zhao, Y. Li, J. Luo, Sintering conversion to porous diopside ceramic from geopolymer fabricated by iron tailings and steel slag, Cer. Int. 51 (12) (2025) 15687–15698, https://doi.org/10.1016/j.ceramint.2025.01.405.
[11] A. Karamanov, L. Arrizza, I. Matekovits, M. Pelino, Properties of sintered glass-ceramics in the diopside–albite system, Cer. Int. 30 (8) (2004) 2129–2135, https://doi.org/10.1016/j.ceramint.2003.11.019.
[12] J. Feng, D. Wu, M. Long, K. Lei, Y. Sun, X. Zhao, Diopside glass-ceramics were fabricated by sintering the powder mixtures of waste glass and kaolin, Cer. Int. 48 (18) (2022) 27088–27096, https://doi.org/10.1016/j.ceramint.2022.06.020.
[13] H. King, Diopside. a pyroxene mineral found in igneous and metamorphic rocks, Retrieved 22 July 2024, from, https://geology.com/minerals/diopside.shtml, 2018.
[14] S. Zhang, Y. Zhang, T. Wu, Effect of Cr_2O_3 on the crystallization behavior of synthetic diopside and characterization of Cr-doped diopside glass ceramics, Cer. Int. 44 (9) (2018) 10119–10129, https://doi.org/10.1016/j.ceramint.2018.02.231.
[15] J. Kirchherr, D. Reike, M. Hekkert, Conceptualizing the circular economy: an analysis of 114 definitions, Resour. Conserv. Recycl. 127 (2017) 221–232, https://doi.org/10.1016/j.resconrec.2017.09.005.
[16] S. Jørgensen, L.J.T. Pedersen, The circular rather than the linear economy, in: S. Jørgensen, L.J.T. Pedersen (Eds.), Curatori. Sustainable Business Model Innovation, Springer International Publishing, Chamistry, 2018, pp. 103–120, https://doi.org/10.1007/978-3-319-91971-3_8.
[17] R.A. Sheldon, M.L. Bode, S.G. Akakios, Metrics of green chemistry: waste minimization, current opinion in green sustain, Chemistry 33 (2022) 100569, https://doi.org/10.1016/j.cogsc.2021.100569.
[18] R. Arletti, S. Conte, C. Zanelli, M. De Iuliis, D. Di Giuseppe, V. Scognamiglio, D. Malferrari, M. Dondi, A.F. Gualtieri, Recycling the product of thermal inertization of man-made vitreous fibres for the manufacture of stoneware tiles, Waste Biomass. Valor. 14 (5) (2023) 1721–1736, https://doi.org/10.1007/s12649-022-01959-8.
[19] S.H. Park, Types and health hazards of fibrous materials used as asbestos substitutes, Saf. Health Work 9 (3) (2018) 360–364, https://doi.org/10.1016/j.shaw.2018.05.001.
[20] WHO, Determination of airborne fibre number concentrations. A recommended method, by phase contrast optical microscopy (Membrane Filter Method) (1997).
[21] Ref Regulation (EC) No 1272/2008 of the European Parliament and Council (2008).
[22] European Patent EP 22153845.7 “apparatus for treating waste containing mineral wool“. Filing date , 2022.
[23] M. Gemmi, E. Mugnaioli, T.E. Gorelik, U. Kolb, L. Palatinus, P. Boullay, S. Hovmöller, J.P. Abrahams, 3D Electron diffraction: the nanocrystallography revolution, ACS Cent. Sci. 5 (2019) 1315–1329.
[24] B.H. Toby, EXPGUI, a graphical user interface for GSAS, Appl. Cryst. 34 (2) (2001) 210–213, https://doi.org/10.1107/S0021889801002242.
[25] A.C. Larson, R.B. Von Dreele, GSAS Report LAUR, (1994) 86–748.
[26] M. Cameron, S. Sueno, C.T. Prewitt, J.J. Papike, High-temperature crystal chemistry of acmite, diopside, hedenbergite, jadeite, spodumene, and ureyite, Am. Min. 58 (1973) 594–618.
[27] S. Zertani, L.F. Morales, L. Menegon, Omphacite breakdown: nucleation and deformation of clinopyroxene-plagioclase symplectites, Contr. Min. Petr. 179 (5) (2024) 44, https://doi.org/10.1007/s00410-024-02125-0.
[28] G.J. Redhammer, G. Tippelt, G. Amthauer, G. Roth, Structural and 57Fe Mössbauer spectroscopic characterization of the synthetic $NaFeSi_2O_6$ (aegirine) – $CaMgSi_2O_6$ (diopside) solid solution series, Z. Kristallogr. 227 (2012) 396–410, https://doi.org/10.1524/zkri.2012.1514.
[29] N. Morimoto, J. Fabries, A.K. Ferguson, I.V. Ginzburg, M. Ross, F.A. Seifert, J. Zussman, K. Aoki, G. Gottardi, Nomenclature Pyroxenes. Min. Mag. 52 (1988) 535–550.
[30] Y. Hu, B. Kiefer, A. Plonka, J.B. Parise, J.S. Zhang, M.H. Manghnani, B.N. Sahu, P. K. Dera, Compressional behavior of end-member and aluminous iron-bearing diopside at high pressure from single-crystal X-ray diffraction and first principles calculations, Phys. Chem. Mineral. 46 (10) (2019) 977–986, https://doi.org/10.1007/s00269-019-01056-8.
[31] R. Titorenkova, V. Kostov-Kytin, T. Dimitrov, Synthesis, phase composition and characterization of Co-diopside ceramic pigments, Cer. Int. 48 (24) (2022) 36781–36788, https://doi.org/10.1016/j.ceramint.2022.08.242.
[32] M.B. Sedel’nikova, V.M Pogrebenkov, Production of ceramic pigments with wollastonite and diopside structures using nepheline sludge, Glass Cer 64 (9) (2007) 363–365, https://doi.org/10.1007/s10717-007-0091-7.
[33] W.Y. Zhang, H. Gao, Y. Xu, Sintering and reactive crystal growth of diopside–albite glass–ceramics from waste glass, J. European Cer. Soc. 31 (9) (2011) 1669–1675, https://doi.org/10.1016/j.jeurceramsoc.2011.02.037.
[34] T. Nonami, S. Tsutsumi, Study of diopside ceramics for biomaterials, J. Mat. Sci. Materials in Med. 10 (8) (1999) 475–479, https://doi.org/10.1023/A:1008996908797.
[35] N. Namvar, E. Salahinejad, A.H. Saberi, M.J. Baghjeghaz, L. Tayebi, D. Vashaee, Toward reducing the formation temperature of diopside via wet-chemical synthesis routes using chloride precursors, Cer. Int. 43 (16) (2017) 13781–13785, https://doi.org/10.1016/j.ceramint.2017.07.094.
[36] B.N. Sherikar, B. Sahoo, A.M. Umarji, One-step synthesis of diopside ($CaMgSi_2O_6$) ceramic powder by solution combustion method, Adv. Powder Tech. 31 (8) (2020) 3492–3499, https://doi.org/10.1016/j.apt.2020.06.037.
[37] A. Kazemi, M. Abdellahi, A. Khajeh-Sharafabadi, A. Khandan, N. Ozada, Study of in vitro bioactivity and mechanical properties of diopside nano-bioceramic synthesized by a facile method using eggshell as raw material, Mat. Sci. and Eng. C 71 (2017) 604–610, https://doi.org/10.1016/j.msec.2016.10.044.
[38] S. Palakurthy, K.V. Reddy, S. Patel, P.A. Azeem, A cost effective SiO_2–CaO–Na_2O bio-glass derived from bio-waste resources for biomedical applications, Progress Biomat. 9 (4) (2020) 239–248, https://doi.org/10.1007/s40204-020-00145-0.
[39] R. Choudhary, S.K. Venkatraman, I. Bulygina, F. Senatov, S. Kaloshkin, N. Anisimova, M. Kiselevskiy, M. Knyazeva, D. Kukui, F. Walther, S. Swamiappan, Biomineralization, dissolution and cellular studies of silicate bioceramics prepared from eggshell and rice husk, Mat. Sci. and Eng. C 118 (2021) 111456, https://doi.org/10.1016/j.msec.2020.111456.
[40] S.K. Venkatraman, M. Saraswat, R. Choudhary, F. Senatov, S. Kaloshkin, S. Swamiappan, Photocatalytic degradation of methylene blue dye by calcium-and magnesium-based silicate ceramics, Chem. Select 5 (39) (2020) 12198–12205, https://doi.org/10.1002/slct.202003046.